electronics

Article

Experimental Study on Human Kinetic Energy Harvesting with Wearable Lifejackets to Assist Search and Rescue

Jeffrey To and Loulin Huang *

School of Engineering, Computer and Math. Sciences, Auckland University of Technology, 6 St. Paul Street, Auckland 1010, New Zealand; jeffrey.to@autuni.ac.nz
* Correspondence: loulin.huang@aut.ac.nz; Tel.: +064-9-921-9999 (ext. 6708)

Abstract: This study explores the integration of a human kinetic energy-harvesting mechanism into lifejackets to address the energy needs of aid search and rescue operations in aquatic environments. Due to the limited data on the movement patterns of drowning individuals, a human motion model has been developed to identify optimal design parameters for energy harvesting. This model is developed from computer vision analysis of underwater footage and motion capture laboratory experiments and is used to quantify the potential for power generation. The field testing experiment is conducted underwater, replicating the environment used for footage collection and analysis for the modelling. During the field testing, the participant wears a lifejacket integrated with the energy-harvesting device. Field testing data are then collected to verify the model. The efficacy of this approach is demonstrated with observed power outputs ranging from 0 mW to 754 mW in simulations and experiments. Despite challenges such as the "dead zone" in a drowning person's motion, the success of the experiments underscores the potential of the proposed energy-harvesting mechanism to efficiently harness the kinetic energy generated by a drowning person's movements. This study contributes to the development of sustainable, energy-efficient solutions for search and rescue operations, particularly in remote and challenging aquatic environments.

Keywords: energy harvesting; lifejacket; search and rescue; motion capture; drowning

Citation: To, J.; Huang, L. Experimental Study on Human Kinetic Energy Harvesting with Wearable Lifejackets to Assist Search and Rescue. *Electronics* **2024**, *13*, 4059. https://doi.org/10.3390/electronics13204059

Academic Editors: Moshe Averbukh, Shailendra Rajput and Francesco Giuseppe Della Corte

Received: 27 August 2024
Revised: 3 October 2024
Accepted: 9 October 2024
Published: 15 October 2024

1. Introduction

Water Safety New Zealand underscores drowning as the fourth most prevalent cause of accidental death in the nation, documenting 74 and 82 drowning fatalities in 2020 and 2019, respectively [1,2]. Studies reveal that drowning constitutes 82% of the total 320 water-related fatalities recorded between 2010 and 2017, with only 1% attributed to hypothermia [3]. New Zealand ranks eighth among OECD countries in drowning rates per 100,000 individuals [4]. The execution of search and rescue missions for drowning victims poses formidable challenges, especially in remote and hazardous settings. Recently, wearable and IoT technology has emerged as a promising avenue for enhancing the safety of individuals participating in aquatic endeavours [5]. However, most IoT-equipped lifejackets rely on batteries with limited lifespans. Since lifejackets are often not used frequently, users may overlook checking battery levels before use, further complicating matters in emergency situations. Although providing power to the lifejacket alone does not directly reduce drowning rates, it is critical for enabling lifesaving IoT features to function over longer periods.

To address the limitations of a short battery life, attention has shifted to energy harvesting—a process that converts ambient energy into electrical power. The integration of a small battery with an energy harvester offers a more reliable power supply. This approach not only supports the current IoT features but also creates possibilities for future enhancements that may require more power. By extending the operational life of the devices, energy harvesting enables further research into additional lifesaving features that could increase the efficacy of lifejackets in search and rescue missions.

The movements of a drowning victim's limbs generate significant kinetic energy, presenting a promising avenue for harnessing sustainable power for these devices. This study delves into the experimental exploration of human body dynamics in water environments and their relation to energy (power) harvesting. Underwater footage, captured while participants wore lifejackets, allowed for data extraction through computer vision analysis. Employing a DC motor as an energy-harvesting device (power generator), the investigation demonstrated a peak power output of 754 mW, which was harnessed through the movement of one side of the participant's hip joint.

Given the limited availability of drowning motion data, previous research has concentrated on developing methods for capturing this motion. Two distinct approaches are employed for data collection: the first utilised infrared cameras in AUT's Motion Capture Lab, while the second involved underwater data collection using computer vision technology. A motion model is then developed based on the collected data, and calculations are conducted to estimate the potential for energy harvesting. In this study, the field test is conducted at a local swimming facility, where a participant engages in ladder-climbing motions underwater while outfitted with both the energy-harvesting device setup and lifejackets. Following data collection, underwater video footage is processed via computer vision technology, enabling the recording and exportation of participants' joint coordinates for subsequent analysis. Energy-harvesting calculations are then conducted based on those data. This methodology possesses inherent adaptability, promising seamless integration with alternative motion capture techniques and energy-harvesting devices for future research and development.

The paper is organised as follows: Section 2 details the materials and methods adopted in the experiments. Section 3 presents the experimental results. Section 4 discusses the findings of the experiments, and conclusions are given in Section 5.

2. Energy-Harvesting Mechanism and Device

2.1. Common IoT Device Power Requirement

In order to integrate an IoT with a lifejacket, sensors, a Microcontroller Unit (MCU), an Analog-to-Digital Converter (ADC), a DC-DC converter, a power-management unit, a wireless transmission module, and an interface for human–computer interaction are required [6]. Table 1 lists the requirements of voltage, current, and power of several typical parts in an IoT system.

Table 1. Summary of power consumption for various components.

Part	Category	Size	Voltage [V]	Current [mA]	Power [mW]
Sensors	Thermistor [7]	50 mm × 10 mm	10	0.00079–0.00134	0.01
	Pressure sensor [8]	65 mm × 65 mm × 0.5 mm	1.5	0.55	0.825
MCU	Active mode	3 mm × 3 mm × 0.8 mm	3	4	0.001
	Sleep mode [9]	3 mm × 3 mm × 0.8 mm	3	0.150	0.003
ADC	Signal conversion [10]	3 mm × 3 mm	3	1.2	0.003
DC-DC energy storage	Power management	2 mm × 2 mm × 0.74 mm	4.2	0.08	0.34
Data transmission	BLE processing	8 mm × 8 mm × 1 mm	3.3	1	0.001
	BLE sleep	8 mm × 8 mm × 1 mm	3.3	0.001	0.0033
	LoRa Rx/Tx	16 mm × 16 mm × 3.5 mm	3.3	33	108.9
	LoRa sense	16 mm × 16 mm × 3.5 mm	3.3	4.2	13.86
	LoRa sleep [11,12]	16 mm × 16 mm × 3.5 mm	3.3	0.0247	0.0815

Table 1. *Cont.*

Part	Category	Size	Voltage [V]	Current [mA]	Power [mW]
Display interface	LED [13]	10 cm^2	3	15	0.02
	Electronic ink	10 cm^2	3	45	0.06
Total					172.448

2.2. Lifejacket

For this experiment, the Hutch-wilco Easy-Fit Inflatable Lifejacket was employed. This lifejacket, renowned for its user-friendly design and reliable performance, features an advanced roll over system and a buoyancy of 170 N [14]. The harvesting device is strategically mounted onto the waist strap of the lifejacket, ensuring ease of use and optimal functionality.

2.3. Energy-Harvesting Mechanism

Figure 1 shows the prototype of the harvesting device mounted on the waist strap of the lifejacket, ensuring optimal placement and functionality. A telescopic linkage, one end of which is affixed to the harvesting device and the other to the thigh strap, facilitates the mechanism's operation. During ladder-climbing motions, as the participant moves their leg up and down, the angle of the linkage adjusts accordingly, thereby rotating the YG2734 motor. This rotational movement generates electrical energy, effectively harnessing the participant's motion to produce power.

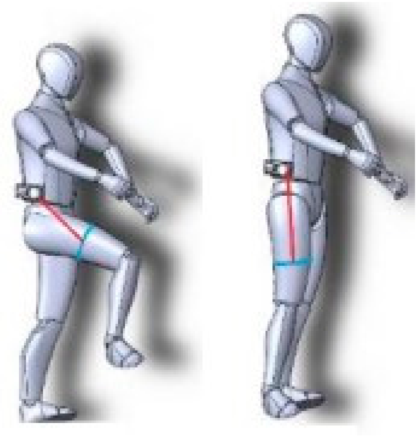

Figure 1. Conceptual design where the energy harvester is located at the waist strap of the lifejacket.

2.4. DC Motor—Energy-Harvesting Device

The generator employed for harvesting purposes in this experiment is the YG2734 12 V DC motor. Characterised by its gear head design with a ratio of 244:1, this motor is ideally suited for the experiment's requirements [15]. Operating at a maximum efficiency speed of 29 RPM with 2.52 Watts, it serves as an excellent testing model. Noteworthy specifications include a torque constant of 840.007 $\text{mN} - \text{m}/\text{AMP}$ and an electromagnetic force (E.M.F) constant of 87.921 $\text{mV}/\text{rad}/\text{s}$, as detailed in the specification sheet in Figure 2. These specifications greatly facilitate both Matlab (R2022b) and manual calculations, enhancing the experiment's precision and reliability.

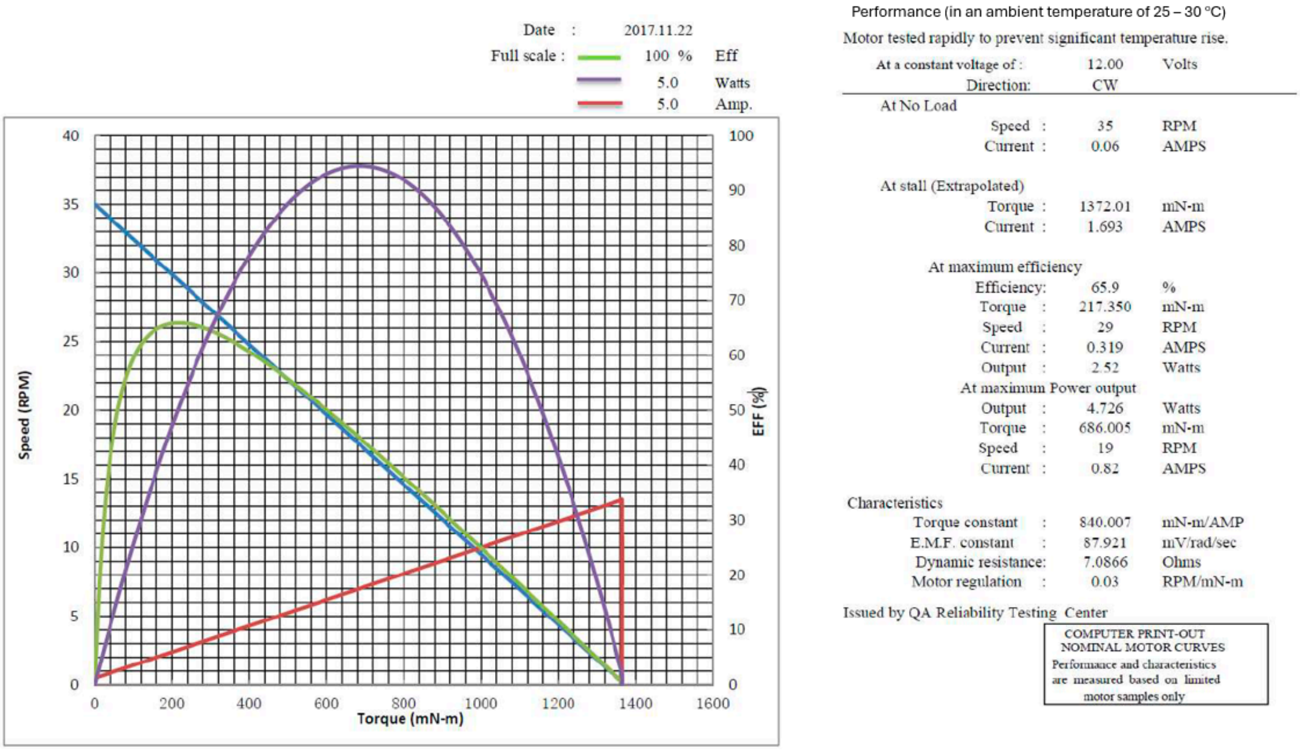

Performance (in an ambient temperature of 25 – 30 °C)

Motor tested rapidly to prevent significant temperature rise.

At a constant voltage of : 12.00 Volts
Direction: CW

At No Load
Speed : 35 RPM
Current : 0.06 AMPS

At stall (Extrapolated)
Torque : 1372.01 mN-m
Current : 1.693 AMPS

At maximum efficiency
Efficiency: 65.9 %
Torque : 217.350 mN-m
Speed : 29 RPM
Current : 0.319 AMPS
Output : 2.52 Watts
At maximum Power output
Output : 4.726 Watts
Torque : 686.005 mN-m
Speed : 19 RPM
Current : 0.82 AMPS

Characteristics
Torque constant : 840.007 mN-m/AMP
E.M.F. constant : 87.921 mV/rad/sec
Dynamic resistance: 7.0866 Ohms
Motor regulation : 0.03 RPM/mN-m

Issued by QA Reliability Testing Center

COMPUTER PRINT-OUT
NOMINAL MOTOR CURVES
Performance and characteristics are measured based on limited motor samples only

Figure 2. Specification details of YG2734 12 V motor [15].

2.5. Electrical Circuit for the Prototype

Figure 3 shows the electrical circuit for the prototype that is used in the experiment. This circuit is designed to harvest kinetic energy by using the YG2734 12 V brushed DC motor. Below is a breakdown of the circuit components and their functions:

1. **Bridge Rectifier**: The motor produces alternating current (AC) as it rotates in both directions. A bridge rectifier, made up of four diodes (D1, D2, D3, and D4), converts the AC into direct current (DC). This ensures a consistent output polarity, regardless of motor direction.
    - In one direction, current flows through D1 and D2.
    - In the opposite direction, it flows through D3 and D4.
    - This converts the AC to a pulsating DC waveform.
2. **INA219 Current Sensor Module**: The INA219 is a current-sense amplifier designed by Texas Instruments. It is used to monitor current by measuring the voltage across a low-side or high-side shunt resistor. The chip amplifies this small voltage differential, which is proportional to the current, and outputs a corresponding signal that can be read by microcontrollers or other systems. More details of the module are shown in the experimental setup.
    - High accuracy with low offset and drift.
    - Operates with a wide common-mode voltage range (from −0.3 V to 26 V).
    - Low power consumption.
3. **Arduino UNO R3**: The Arduino UNO R3 is a widely used microcontroller board based on the ATmega328P microcontroller. It is popular for prototyping and educational purposes due to its simplicity and large community support. The UNO R3 features the following:
    - Fourteen digital input/output pins, six of which can be used as PWM outputs.
    - Six analogue input pins.
    - A 16 MHz quartz crystal for clocking.
    - A USB connection for programming and power.

4. **12 V 1.2 W Automotive Globe**: The 12 V 1.2 W automotive globe is a small incandescent light bulb commonly used in vehicles for indicator or dashboard lights. In this circuit, it serves as an electrical load, meaning it consumes the electrical power generated by the DC motor. The globe provides a simple way to measure the performance of the system because the current flowing through it can be monitored, and its brightness can be used as a visual indicator of the power output. Its low power rating makes it suitable for small-scale testing setups like the one you are using with the DC motor and INA219.

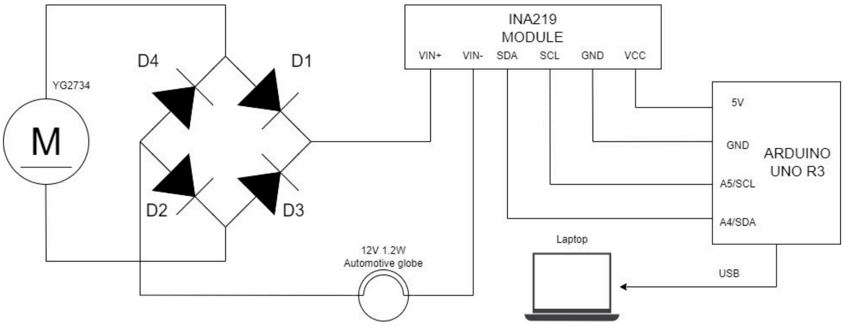

Figure 3. Circuit diagram for the experiment's prototype.

2.6. Future Electrical Circuit Consideration

Although the prototype used in this research focuses only on energy harvesting and does not require the full circuit, the electrical circuit needed to harvest and store the energy has been considered. A diagram of the draft circuit is shown in Figure 4. The battery in this circuit can be replaced with other energy-storage devices, such as a supercapacitor. Additional sensors or equipment can be connected to the voltage regulator or the energy storage unit to meet different system needs.

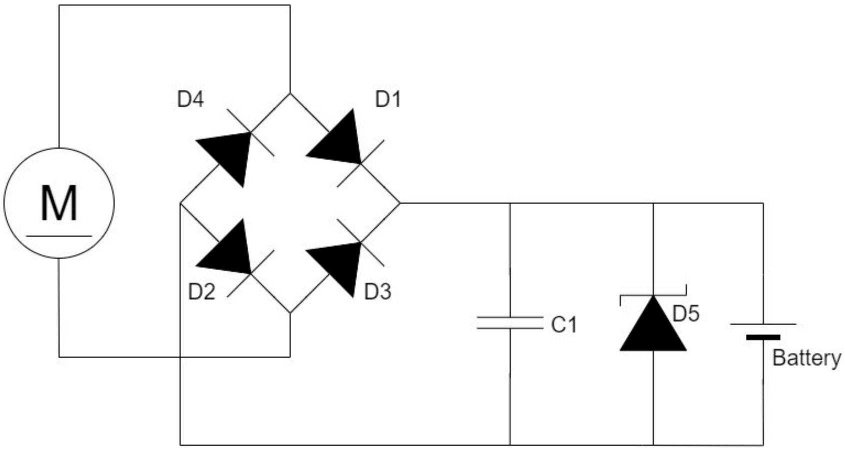

Figure 4. Circuit diagram consideration for the DC motor as the energy harvester of the future.

Below is a breakdown of the circuit components and their functions:

1. **Smoothing Capacitor (C1)**: Capacitor C1 smooths the pulsating DC output from the rectifier by charging during voltage peaks and discharging during troughs, providing a more stable DC output. An 8200 µF/25 V capacitor is suggested but the actual value should be reconsidered according to the production design.
2. **Voltage Regulation and Safety**: A Zener diode (D5) protects the circuit from overvoltage when the motor spins too fast, clamping the voltage to a safe level (5 V or 12 V). The suggested value for the Zener diode is 15 V with a power rate of 2 W, but

the actual value should be reconsidered during the production design stage. A charge controller can also be used to ensure the battery is not being overcharged.

3. **Energy Storage**: The harvested energy is stored in either a supercapacitor or a rechargeable battery, depending on the requirements:
    - **Supercapacitors**: ideal for rapid charge and discharge, with longer lifespans and better short-term energy storage.
    - **Batteries**: Higher energy density, suitable for long-term storage but with fewer charge–discharge cycles.

3. Power-Harvesting Modelling

3.1. Motion Analysis

In the previous study, the ladder-climbing motion pattern of a simulated drowning individual was captured utilising two distinct methods [16]. Firstly, infrared cameras within a motion capture laboratory were employed while the participant was suspended from a frame to simulate floating [17]. Secondly, computer vision analysis was conducted on underwater video footage featuring the participant [18,19]. The data obtained from these recordings are then processed manually with Matlab.

In manual calculations, the translational motion within the global coordinate system ($o - xyz$) is determined by treating the human body as a rigid object as shown in Figure 5. $O_b - x_b y_b z_b$ and $G - \hat{x}\hat{y}\hat{z}$ are the body coordinate frame and the body coordinate formed by COG principal axes, respectively [20].

$$M_{(sub)}\ddot{S}_G = F \tag{1}$$

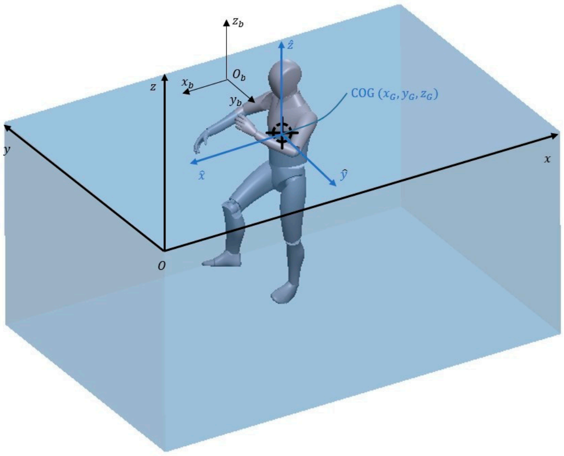

Figure 5. Dynamic model of human performing ladder-climbing motion.

In accordance with Newton's second law, where $M_{(sub)}$ is the mass of the body segment, $s_G = [x_G\ y_G\ z_G]^T$ is the displacement vector of the subject's centre of gravity (COG), and F denotes the resultant external force including gravity force F_G, normal drag force F_n, tangential drag force F_t, and added mass force F_a, as shown in Figure 6. Each of them is the resultant force acting on the corresponding segment in the model. The body segments are shown in Figure 7.

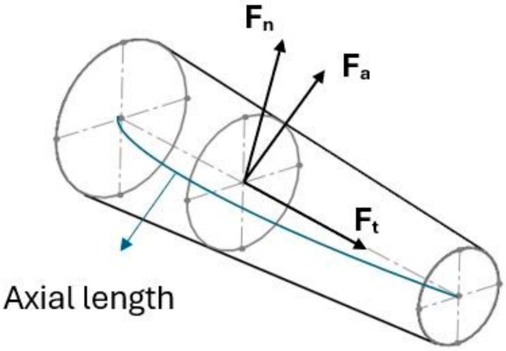

Figure 6. Illustration of the fluid forces acting on the truncated elliptical cone—limb.

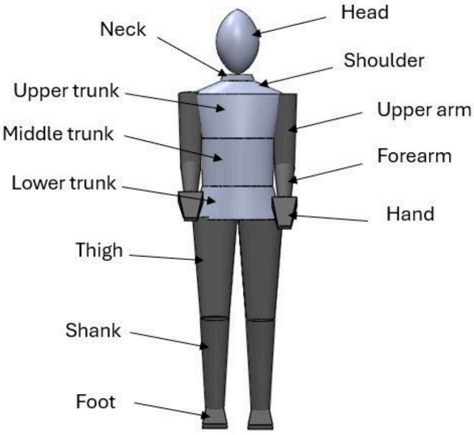

Figure 7. Body segments for motion analysis.

The rotational motion of the subject can be described with the Euler equations in a principle axes coordinate system:

$$\begin{aligned} J_{\hat{x}}\dot{\omega}_{\hat{x}} + (J_{\hat{z}} - J_{\hat{y}})\omega_{\hat{y}}\omega_{\hat{z}} + \dot{J}_{\hat{x}}\omega_{\hat{x}} = M_{\hat{x}} J_{\hat{y}}\dot{\omega}_{\hat{y}} + (J_{\hat{x}} - J_{\hat{z}})\omega_{\hat{x}}\omega_{\hat{z}} + \dot{J}_{\hat{y}}\omega_{\hat{y}} \\ = M_{\hat{y}} J_{\hat{z}}\dot{\omega}_{\hat{z}} + (J_{\hat{y}} - J_{\hat{x}})\omega_{\hat{x}}\omega_{\hat{y}} + \dot{J}_{\hat{z}}\omega_{\hat{z}} = M_{\hat{z}} \end{aligned} \tag{2}$$

where $\hat{x}$, $\hat{y}$, $\hat{z}$ are the three principal axes of inertia of the human body; J_i and $\omega_\iota(i = \hat{x}\ \hat{y}\ \hat{z})$ are the moment of inertia and the angular velocity of the human body about the ι axis, and $M_\iota(i = \hat{x}\ \hat{y}\ \hat{z})$ indicates the total external moment about the ι axis applied to the subject. Due to the relative movements of the subjects during the ladder-climbing motion, the moment of inertia around each principal axis of the subject is not constant, refer to Equation (2). The details of the motion analysis manual calculation can be found in a previous study, "An approach to model human kinetic energy harvesting with wearable lifejacket to assist search and rescue" [16].

3.2. Power Generation by the Harvesting System

As shown in Figure 8, the hip angle θ is defined as the positive clockwise displacement of the thigh from the hip, and the angular velocity of the hip joint is $\dot{\theta}$, and the gear head has a ratio of μ. If the energy harvester (generator) is placed closer to the waist above the hip joint, the rotation angle of the energy harvester is lower. To maximise the rotation angle, the harvester is placed at the hip joint where $\dot{\theta}_g = \mu\dot{\theta}$ is the angular velocity of the generator shaft.

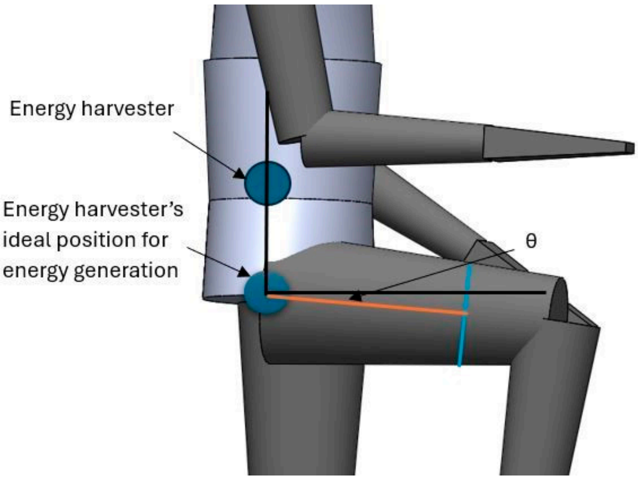

Figure 8. A sketch of the harvesting system with the ideal position of the energy harvester.

During the ladder-climbing motion, the generator produces a voltage E, which is as follows:

$$E = K_g \dot{\theta}_g$$

where K_g is the back electromotive force constant of the generator. The electricity power, denoted by P_g, can be calculated as follows:

$$P_g = \frac{E^2}{R_i + R_o} = \frac{{K_g}^2 \dot{\theta}_g{}^2}{R_i + R_o} = C_g \dot{\theta}_g{}^2 = C_e \theta^2$$

where R_o is the external resistive load, R_i is the internal resistance of the generator, C_g is the electromagnetic damping coefficient of the generator, and C_e is the electrical damping coefficient of the entire harvesting system as shown below. C_e is then derived from the abovementioned equations as follows:

$$C_e = C_g \mu^2 = \frac{{K_g}^2 \mu^2}{R_i + R_o} \tag{3}$$

Figure 9 shows the transmission diagram of the harvesting system with the parameters. The output power, denoted by P_{out} and representing the energy dissipation of the external resistive load R_o, is given as follows:

$$P_{out} = \frac{{K_g}^2 \mu^2 \dot{\theta}^2 R_o}{(R_i + R_o)^2}$$

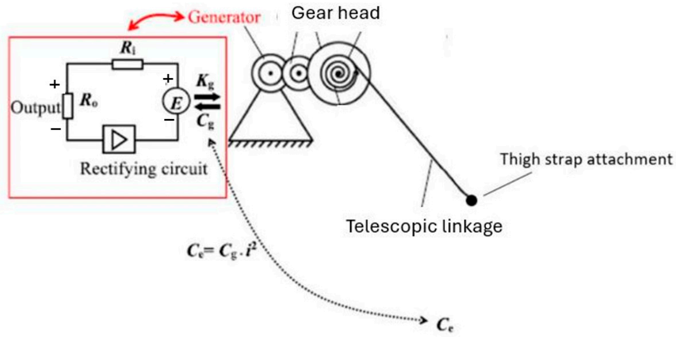

Figure 9. Transmission diagram of the energy-harvesting system.

The output power of each half of the harvesting system depends on the hip joint's angle of rotation and the external load resistance. As a result, changing the external load resistance results in a change in output power and damping coefficient, with the output power reaching its maximum value of $\frac{{K_g}^2\mu^2\dot{\theta}^2}{4R_i}$ when $R_i = R_o$. According to Equation (3), the electrical damping coefficient of the lower limb exoskeleton (C_e) is determined by the external resistive load R_o for a given generator.

3.3. Motion Data Collection

The data collection phase commences within a controlled swimming pool environment. A participant dons the inflatable lifejacket and executes ladder-climbing motions underwater. Throughout the experiment, footage of the participant's movements is captured utilising an underwater camera Kaiser Baas X350 Action Cam with 4K capabilities. Subsequently, it is subjected to analysis using MediaPipe (v0.10.15), as illustrated in Figure 10. This software facilitates the extraction of pertinent data, allowing for the detailed examination of the participant's motion patterns and energy-harvesting dynamics.

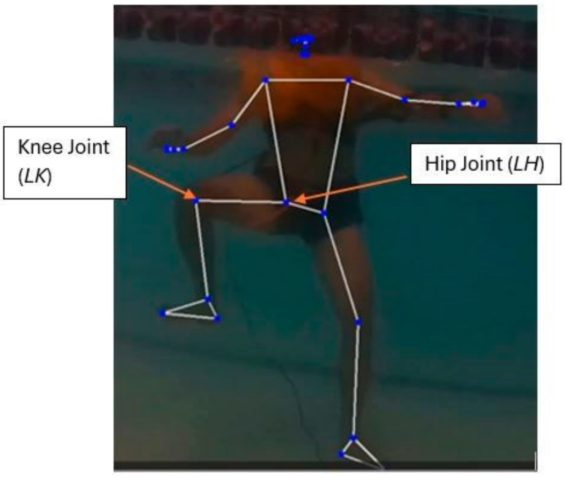

Figure 10. Screenshot from the underwater video with computer vision and MediaPipe analysis.

MediaPipe is an open-source framework developed by Google, offering a comprehensive suite of tools and building blocks geared towards applications with perceptual computing capabilities.

The MediaPipe analysis yielded data for 33 distinct points [21]. Within the scope of this study, specific focus was placed on points 24 and 26, corresponding to the hip and knee joints respectively. Notably, the x, y, z coordinates of these points are expressed as ratios relative to the video's dimensions, which stand at 1920 pixels in width and 1080 pixels in height. Notably, the origin point is situated at the top left corner of the video frame.

Figure 11 provides a visual representation of the collected data, offering insight into the spatial distribution and movement patterns of the tracked points. Given that the video footage was captured at a rate of 30 frames per second, the corresponding time interval between frames is approximately 0.0333 s.

The movement of the whole body is analysed, and the movement of the limbs is the most obvious. Next, we determine which movement would give more potential for energy harvesting without creating excessive resistance to the wear.

The potential for energy harvesting from the participant's limb movements was calculated using the formula for rotational kinetic energy:

$$E_k = \frac{1}{2}I\omega^2$$

where E_k is the kinetic energy, I is the moment of inertia, and ω is the angular velocity. The moment of inertia for the thigh is generally larger than that of the arm, with typical values ranging from 0.1 to 0.2 kg·m² for the thigh and 0.02 to 0.03 kg·m² for the arm. Given that the energy potential is directly proportional to both the moment of inertia and the square of the angular velocity, the thighs, with their higher inertia and relatively high angular velocity, emerge as a more promising source of energy.

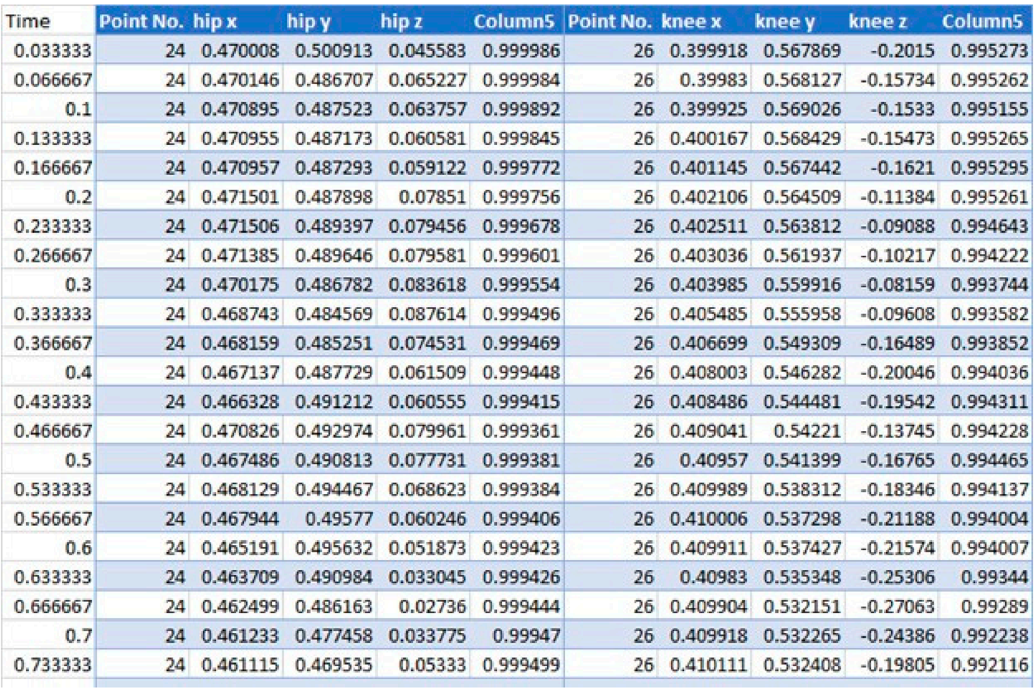

Time	Point No.	hip x	hip y	hip z	Column5	Point No.	knee x	knee y	knee z	Column5
0.033333	24	0.470008	0.500913	0.045583	0.999986	26	0.399918	0.567869	-0.2015	0.995273
0.066667	24	0.470146	0.486707	0.065227	0.999984	26	0.39983	0.568127	-0.15734	0.995262
0.1	24	0.470895	0.487523	0.063757	0.999892	26	0.399925	0.569026	-0.1533	0.995155
0.133333	24	0.470955	0.487173	0.060581	0.999845	26	0.400167	0.568429	-0.15473	0.995265
0.166667	24	0.470957	0.487293	0.059122	0.999772	26	0.401145	0.567442	-0.1621	0.995295
0.2	24	0.471501	0.487898	0.07851	0.999756	26	0.402106	0.564509	-0.11384	0.995261
0.233333	24	0.471506	0.489397	0.079456	0.999678	26	0.402511	0.563812	-0.09088	0.994643
0.266667	24	0.471385	0.489646	0.079581	0.999601	26	0.403036	0.561937	-0.10217	0.994222
0.3	24	0.470175	0.486782	0.083618	0.999554	26	0.403985	0.559916	-0.08159	0.993744
0.333333	24	0.468743	0.484569	0.087614	0.999496	26	0.405485	0.555958	-0.09608	0.993582
0.366667	24	0.468159	0.485251	0.074531	0.999469	26	0.406699	0.549309	-0.16489	0.993852
0.4	24	0.467137	0.487729	0.061509	0.999448	26	0.408003	0.546282	-0.20046	0.994036
0.433333	24	0.466328	0.491212	0.060555	0.999415	26	0.408486	0.544481	-0.19542	0.994311
0.466667	24	0.470826	0.492974	0.079961	0.999361	26	0.409041	0.54221	-0.13745	0.994228
0.5	24	0.467486	0.490813	0.077731	0.999381	26	0.40957	0.541399	-0.16765	0.994465
0.533333	24	0.468129	0.494467	0.068623	0.999384	26	0.409989	0.538312	-0.18346	0.994137
0.566667	24	0.467944	0.49577	0.060246	0.999406	26	0.410006	0.537298	-0.21188	0.994004
0.6	24	0.465191	0.495632	0.051873	0.999423	26	0.409911	0.537427	-0.21574	0.994007
0.633333	24	0.463709	0.490984	0.033045	0.999426	26	0.40983	0.535348	-0.25306	0.99344
0.666667	24	0.462499	0.486163	0.02736	0.999444	26	0.409904	0.532151	-0.27063	0.99289
0.7	24	0.461233	0.477458	0.033775	0.99947	26	0.409918	0.532265	-0.24386	0.992238
0.733333	24	0.461115	0.469535	0.05333	0.999499	26	0.410111	0.532408	-0.19805	0.992116

Figure 11. Sample of some of the data collected from the experiment where Point No. 24 is the hip joint and Point No. 26 is the knee joint.

Utilising the two sets of coordinates, calculations were conducted to determine both the angle and angular speed of the thigh's vertical movement. Analysis revealed that the range of motion spans approximately 80 to 90 degrees, showcasing the extent of flexibility exhibited during the experimental task. Moreover, the maximum angular speed observed reached 13 degrees per second, highlighting the dynamic nature of the movement. For visual reference, Figures 12 and 13 illustrates the computed angle and angular speed profiles, providing insight into the temporal evolution of the thigh's vertical motion throughout the experiment.

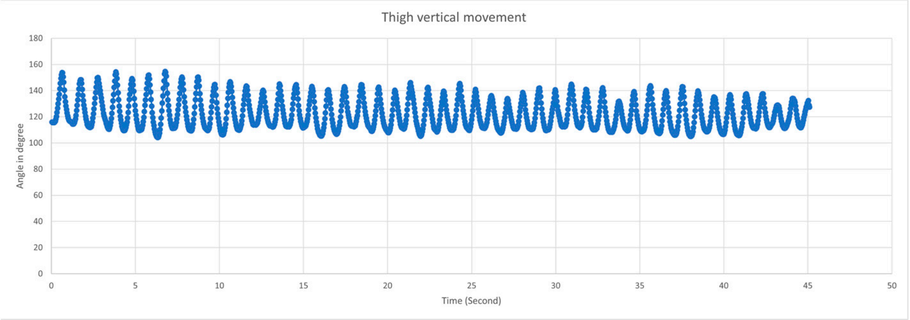

Figure 12. The hip angle changes over time during the ladder-climbing motion.

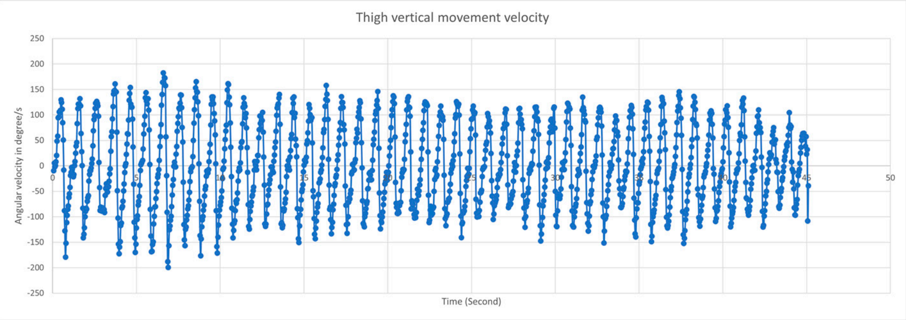

Figure 13. The angular speed of the hip angle during the ladder-climbing motion.

3.4. Energy-Harvesting Modelling

To accurately input the hip joint's angle from motion analysis into Matlab, the coordinates of the hip joint and knee joint collected from motion analysis's data are used. The hip joint angle over time is calculated outside of Matlab-Simulink, so there is no need to transform the axis orientation to fit into the Matlab environment. Along with the hip joint angle, the angular ratio between the hip joint and the energy harvester is also imported into the simulation.

As illustrated in Figure 14, d_1 represents the distance between the hip joint and energy harvester, while d_2 denotes the distance between the hip joint and the thigh strap. The length of the telescopic linkage is indicated by L. Considering a triangle with sides d_1, d_2, and L and corresponding opposite angles α, β, and γ, we can analyse the relationship between these angles and their angular velocities as the length of side L varies, with d_1 and d_2 remaining constant.

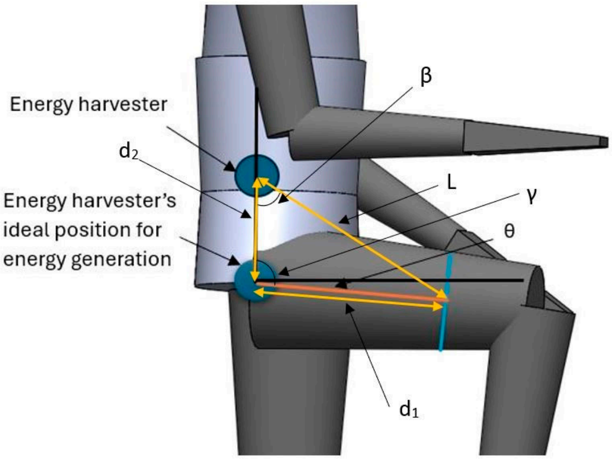

Figure 14. Energy harvester position and angular velocity calculation.

The ratio can be calculated with the equations below:

$$\frac{\omega_\beta}{\omega_\gamma} = \frac{d_2 \cdot \left({d_1}^2 + {d_2}^2 - L^2\right)}{2 \cdot d_1 \cdot L^2} \cdot \frac{\sqrt{1 - {u_\gamma}^2}}{\sqrt{1 - {u_\beta}^2}}$$

where

$$u_\gamma = \frac{{d_1}^2 + {d_2}^2 - L^2}{2 \cdot d_1 \cdot d_2}$$

$$u_\beta = \frac{{d_1}^2 + L^2 - {d_2}^2}{2 \cdot d_1 \cdot L}$$

In this study, the lengths of d_1 and d_2 are held constant, while ω_γ and γ were recorded during the motion capture exercise. Based on these recorded values, ω_β can be derived by rearranging the corresponding equations.

By entering the equations into a spreadsheet and setting d_1 = 0.25 m and d_2 = 0.3 m, the ratio between the hip joint angular velocity and the energy harvester angular velocity can be determined. Table 2 presents an example of the spreadsheet calculations. This table also shows the calculated length of the telescopic linkage, which is a factor for optimising the linkage design to ensure efficient energy harvesting. In Figure 15, the two angular velocities are plotted using data collected through computer vision, with the blue line representing the thigh's vertical angular velocity and the orange line showing the energy harvester's angular velocity. It is clear that the energy harvester's angular velocity remains consistently lower throughout the motion cycle.

Table 2. Example of energy harvester angular velocity data from computer vision.

d_1	d_2	L	u_β	u_γ	Ratio	ω_β deg/s
0.25	0.3	0.477556041	0.839942353	−0.503731818	−0.316443584	
0.25	0.3	0.482078442	0.850067567	−0.532664162	−0.331479765	−19.27656773
0.25	0.3	0.486755388	0.860517675	−0.562872049	−0.346912677	−21.53302119
0.25	0.3	0.491700634	0.871544589	−0.595130089	−0.363105138	−24.69755293
0.25	0.3	0.496911803	0.88313998	−0.629475599	−0.380032591	−28.38317074
0.25	0.3	0.501941534	0.894308554	−0.662968692	−0.396242578	−29.89928637
0.25	0.3	0.507014509	0.90555086	−0.697091416	−0.412468324	−33.0069743
0.25	0.3	0.510753295	0.913822507	−0.722459522	−0.424349405	−26.27326869
0.25	0.3	0.514297551	0.921653119	−0.746679808	−0.435553196	−26.7299137
0.25	0.3	0.516386539	0.926263719	−0.761033721	−0.442130262	−16.60413796
0.25	0.3	0.516545322	0.926614023	−0.762127128	−0.442629386	−1.283643688
0.25	0.3	0.515294469	0.923853851	−0.7535226	−0.438694365	9.944809603
0.25	0.3	0.512750336	0.918235993	−0.736086046	−0.430669272	19.34626547
0.25	0.3	0.510884606	0.914112808	−0.723353872	−0.424765513	13.59654814
0.25	0.3	0.509921022	0.911982205	−0.716796327	−0.421710204	6.85033494
0.25	0.3	0.509139765	0.910254182	−0.711488666	−0.419229875	5.463934082

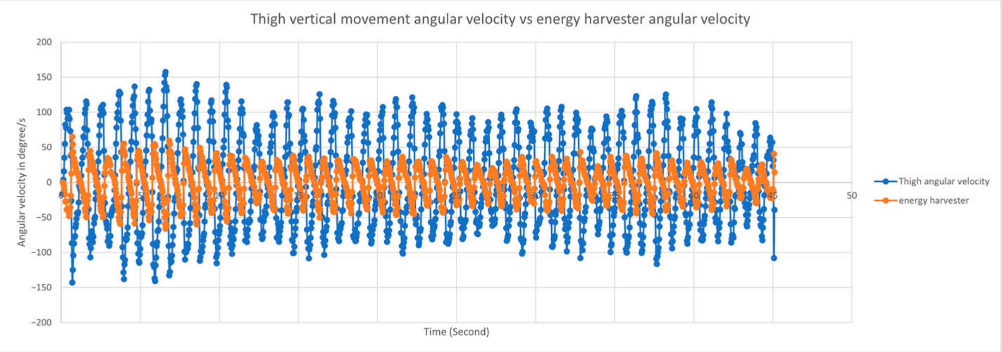

Figure 15. Energy harvester angular velocity vs. hip joint angular velocity—computer vision.

Driven by the motions of the thigh (hip), the motion of the DC motor and the power generated can be calculated manually or with software packages like Matlab. The specifications of the DC motor listed in Figure 2 are critical for the calculation. When choosing another energy harvester, the specifications need to be updated.

Figure 16 displays the power output of the energy harvester from the Matlab simulation, with the maximum power recorded at about 4.25 W and the average peak power ranging from 1.5 W. The power output also displays a clear cycle lasting approximately 1 s. It is important to note that the efficiency of the DC motor is assumed to be 100% for the experiment due to the lack of efficiency information from the specification sheet. The results from the experiment are higher than usual, but they show the limit of the harvesting potential. Table 3 shows the parameters from the specification of the motor are used.

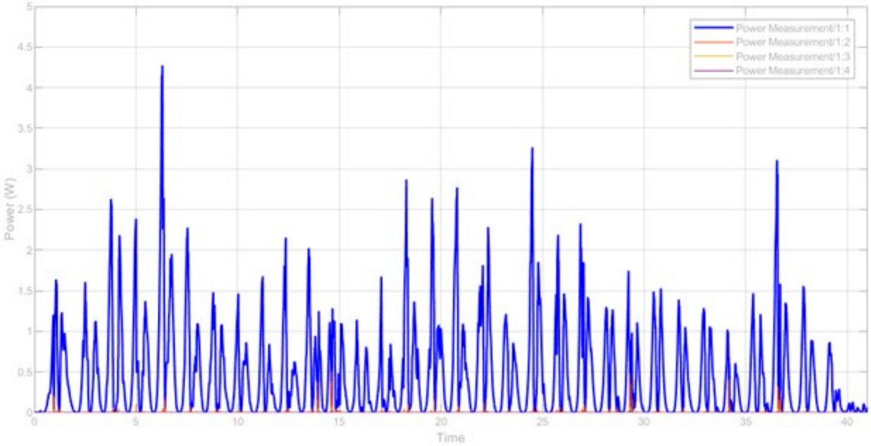

Figure 16. Power output from Matlab calculation with electrical load using computer vision data.

Table 3. Parameters used for the simulation.

Parameter	**Value**	**Unit**
E.M.F constant	87.921	mV/rad/sec
Dynamic resistance (Ri)	7.0866	Ohms
μ	244	-
R_0	120	Ohms
DC motor efficiency	100	%

While an electrical load of 120 Ω is included in the simulation, these outputs are generated without considering efficiency losses or other factors that might affect the actual performance of the energy harvester, but the results provide valuable insights and serve as a useful comparison to the manual calculations conducted earlier. Although other outputs from the DC machine were also captured during the simulation, they are not directly relevant to the main focus of this research and are not discussed at this stage. The specifications of the DC motor show that the maximum efficiency of 65.9%, and the actual efficiency is expected to be much lower with a lower RPM.

4. Experiment Setup and Power Data Collection

4.1. The Electronics Setup

The electronics setup serves the purpose of collecting essential data for this study, encompassing parameters such as bus voltage, shunt voltage, load voltage, current, and power. This setup features the utilisation of the INA219 current sensor and an Arduino Uno board, as depicted in Figure 17.

The INA219 current sensor, developed by Texas Instruments, functions as a high-side current shunt and a power monitor-integrated circuit. Specifically engineered to measure current, voltage, and power within electronic systems, the INA219 finds wide-ranging applications in monitoring and regulating power consumption across various devices and systems. In this experiment, the output of the INA219 sensor is linked to the Arduino board, with the load being a 12 V 1.2 W automotive globe by Enduralight, and the kinetic energy source connected to the YG2734 motor. A rectifier is incorporated between the YG2734 and INA219 to convert alternating current into direct current, ensuring seamless operation.

The Arduino board, in turn, establishes a connection to a computer via USB, facilitating the reading and recording of data. This setup enables comprehensive data collection, which is crucial for the analysis and interpretation of results in this study.

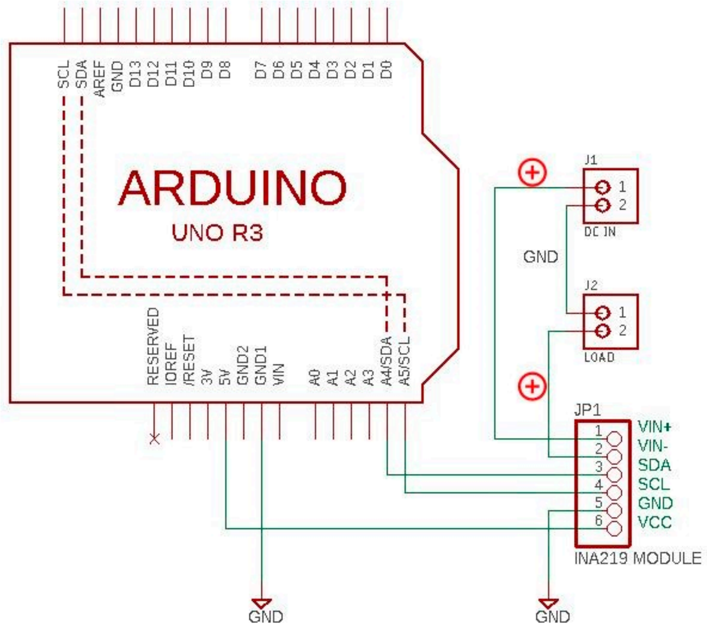

Figure 17. Circuit diagram of the energy harvester [22,23].

4.2. The Software Setup

The Arduino IDE served as the programming platform for configuring the Arduino Uno board. Specifically, the INA219 library, named Adafruit INA219, was utilised. This library provides a readily accessible template designed for measuring purposes, offering flexibility in adjusting voltage and current ranges to enhance accuracy. Upon establishing the connection, real-time results are accessible through the serial monitor.

To facilitate data recording, CoolTerm (version 2.1.0), a serial terminal software, was employed. This software enables the seamless recording of data, subsequently exporting it into a text file for further analysis. Notably, for this study, the data capturing interval was set at 0.1 s, ensuring precise and comprehensive data acquisition throughout the experimental process.

4.3. Power Data Collection

With the priming and configuration of the aforementioned components, the experimental testing phase commences within a controlled swimming pool environment, which is the same as the motion data collection. Figure 18 shows the whole prototype of the energy harvester mechanism.

The participant performs the ladder-climbing motions with a lifejacket integrated with the energy-harvesting device.

Throughout the experiment, a series of 30 s videos are captured, with the participant providing a visual signal to initiate data logging. This signal not only kickstarts the data-logging process but also aids in aligning the data during subsequent processing stages. Within these 30 s footage segments, the participant engages in ladder-climbing motions at a pace mimicking that of an emergency scenario. Concurrently, both the motion of the participant and the corresponding energy-harvesting data are recorded in real time. This synchronised data collection approach facilitates comprehensive analysis and correlation between motion patterns and energy generation.

Figure 18. Energy harvester prototype.

5. Results

5.1. Field Testing—Energy-Harvesting Analysis

Throughout this process, the Arduino UNO communicates with the INA219 to acquire data. Upon receiving a visual signal from the participant, the recording process on the laptop is initiated using the CoolTerm software.

In Figure 19, the observed power generated in the field test reaches its maximum of 754 mW with the average peak value at around 400 mW, while the minimum power recorded was 0 mW. Notably, a distinct "dead zone" is identified when the angular speed is below 2 degrees per second, resulting in negligible power generation. As anticipated, a clear directional relationship between angular speed and power generation is evident. Notably, due to the rectification process, all recorded data are positive.

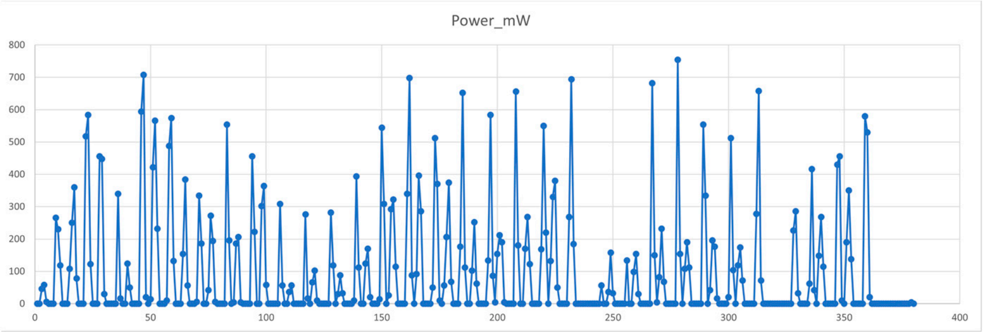

Figure 19. Power (mW) vs. time (s).

Despite the motor being rated at 12 V, the maximum bus voltage observed is 9.08 V, with the maximum shunt voltage reaching 9.95 V and the maximum load voltage reaching 9.09 V. Conversely, the minimum voltage recorded is 0 V. The peak current generated coincided with the moment of maximum power output, reaching 101.1 mA. Figures 20–23 illustrate the temporal evolution of voltages and current fluctuations observed during the experiment, demonstrating their direct association with angular speed.

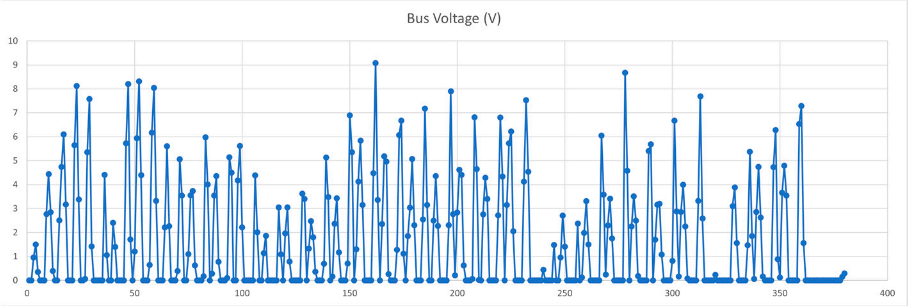

Figure 20. Bus voltage (V) vs. time (s).

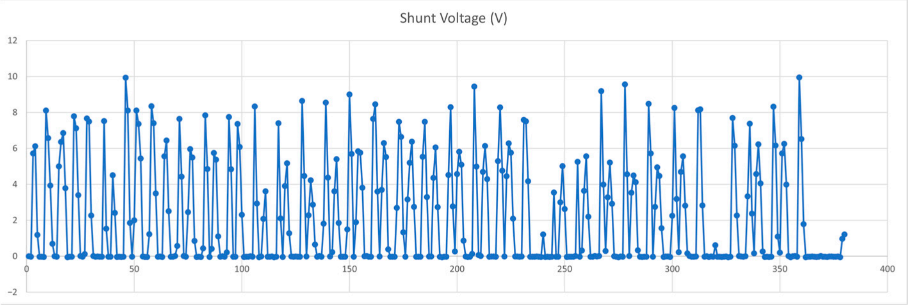

Figure 21. Shunt voltage (V) vs. time (s).

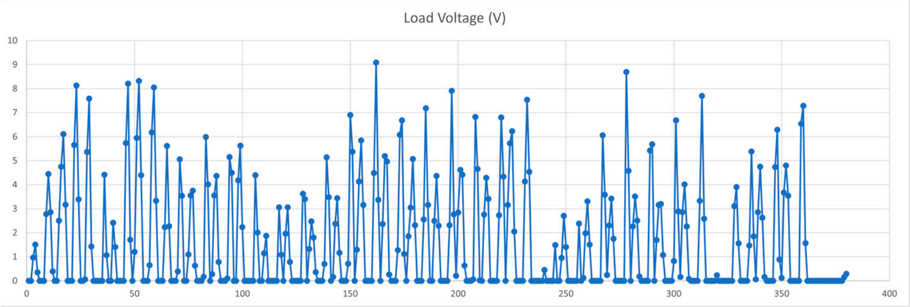

Figure 22. Load voltage (V) vs. time (s).

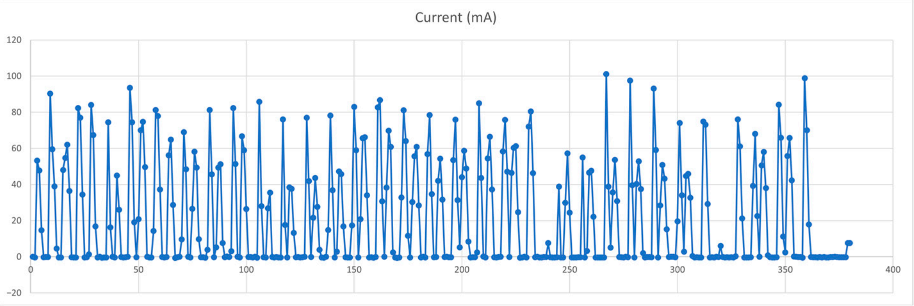

Figure 23. Current (mA) vs. time (s).

Further analysis revealed that the highest power generation occurred during the downward movement of the ladder-climbing motion, specifically when the knee transitioned from its uppermost to its lowermost position. However, upward movements also contributed to power generation, albeit at a reduced level, peaking at 394 mW.

The observed disparities in power generation are found to be directly correlated with the angular speed of the hip movement and, consequently, the angular speed of the generator. Notably, the generator rotates in the same direction as the hip joint, resulting in reversed direction during upward and outward movements. As the knee approached its extremities, the angular speed decreased, eventually reaching 0. As previously mentioned, power generation ceased when the angular speed fell below 2 degrees per second in either direction.

5.2. Energy Harvest Comparison between Experiment and Matlab's Simulation

To calculate the amount of energy harvested from the experiment, the basic energy equation is used, where energy is equal to power multiplied by time:

$$E_h = P_h \cdot t$$

Using this equation and the data obtained from the power output during the experiment, the total energy harvested was calculated. The results of this calculation were collected over a duration of 37.9 s, and the total energy harvested amounted to 3.7584 joules from the experiment.

From the experimental results, the "dead zone" is identified. This zone is added to the Matlab's simulation before the comparison is analysed. According to the Matlab simulation, the sum of the energy harvested over the same duration (37.9 s) was approximately 18.5 joules. The outputs from the experiment and Matlab simulation are shown in Figure 24 where the blue line represents the experimental data and the orange line represents Matlab's simulation data.

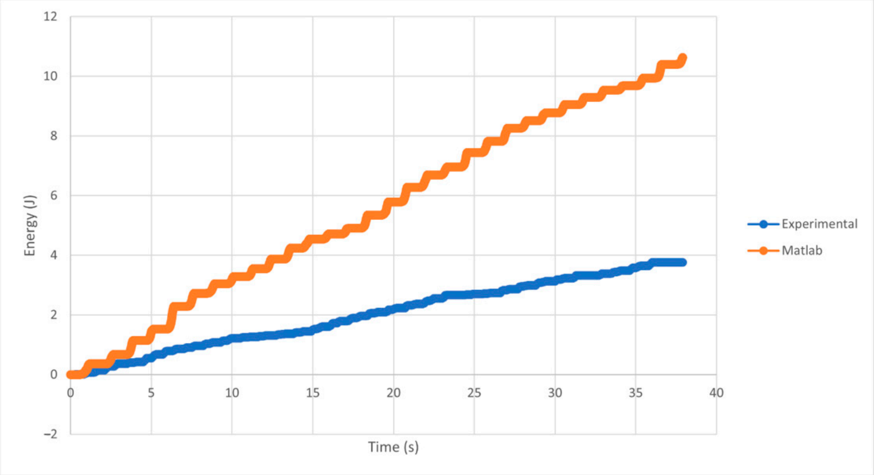

Figure 24. Energy harvested in Matlab simulation.

The equation used to calculate the efficiency of the actual energy harvested in the experiment versus the simulated result is as follows:

$$\frac{Amount\ of\ energy\ generated\ in\ experiment}{Amount\ of\ energy\ generated\ in\ Matlab\ simulation} = 0.3535$$

This calculation yields an efficiency of around 35.4%. One challenge in accurately determining the system's efficiency is the variability in the DC motor's performance when used as a generator. The motor's efficiency changes significantly with different rotational speeds, making it difficult to pinpoint an exact value. However, based on the specification sheet, the DC motor has a maximum efficiency of 65.9% when operating as a motor at 29 RPM. Considering the average peak rotation speed of the energy harvester is at 6.67 RPM, the calculated overall efficiency during the experiment of 35.4% appears reasonable. It is important to note that the motor did not maintain a constant rotational speed throughout the test, and the motor's efficiency fluctuates considerably depending on the speed.

6. Discussion

This study offers a comprehensive examination of integrating motion-harvesting technology with lifejackets for energy generation in aquatic environments.

The observed power generation dynamics underscore the potential of motion-harvesting mechanisms to effectively harness human movement energy. While the average peak power output of 400 mW aligns with the simulated result at 1.2 mW, the experimental calculated maximum output is about 33% of the simulated calculated maximum output. It is important to note that it is assumed that the DC motor has a 100% efficiency during the simulation. The actual output may also be influenced by factors such as the positioning of the harvesting device, particularly above the hip joint, which may result in lesser angular velocity. The identification of a "dead zone" when angular speed falls below 2 degrees per second emphasises the critical role of motion dynamics in optimising energy output while minimising inefficiencies.

Furthermore, the observed directional relationship between angular speed and power generation emphasises the significance of movement directionality in influencing energy-harvesting efficiency. Discrepancies in power generation during different phases of ladder-climbing motions highlight the importance of understanding movement dynamics for designing effective energy-harvesting systems.

7. Conclusions and Future Work

In conclusion, from the experimentation and analysis in this study on human kinetic energy harvesting with wearable lifejackets, the observed power generation patterns demonstrate the potential of energy-harvesting mechanisms proposed. The relationship identified between angular speed and power generation highlights the importance of optimising movement dynamics for effective energy harvesting.

The findings indicate that the downward motion of the thigh yields the highest energy output when the movement reaches peak velocity. However, the natural oscillation of the thigh results in zero angular speeds at fully contracted and extended positions, thereby diminishing energy generation efficiency. While positioning the generator adjacent to the hip joint proves optimal, practical constraints, such as lifejacket design, often hinder this placement. To address this challenge, integrating a gearhead mechanism with the motor can enhance the angular speed of the DC motor, thus augmenting energy-harvesting efficiency.

To improve the existing energy-harvesting mechanism, mechanical rectifiers with flywheels and energy-storage solutions like capacitors or supercapacitors can be utilised to keep energy generation effectiveness at low angular speeds and store energy for a period of time as needed.

A more accurate and precise mathematical model using the D-H parameters method [24] and with a flexible body mechanism is also needed to help optimise the harvester design.

Future research could also encompass a broader range of motion patterns, participant demographics, and environmental conditions to further elucidate the efficacy.

Author Contributions: Conceptualization, J.T. and L.H.; methodology, J.T.; software, J.T.; validation, J.T.; formal analysis, J.T.; investigation, J.T.; resources, J.T.; data curation, J.T.; writing—original draft preparation, J.T.; writing—review and editing, L.H.; visualization, J.T.; supervision, L.H.; project administration, L.H.; funding acquisition, L.H. All authors have read and agreed to the published version of the manuscript.

Funding: This research received no external funding.

Data Availability Statement: Data are contained within the article.

Conflicts of Interest: The authors declare no conflicts of interest.

Abbreviations

The following abbreviations are used in this manuscript:

Ca	The equivalent coefficient of the added mass effect
Ce	the electrical damping coefficient of the entire harvesting system
Cg	The electromagnetic damping coefficient of the generator
dl	The thickness of a thin elliptical plate
$\mathbf{e}$	The unit vectors along the minor and major axis of a thin elliptical plate
E	The generator produced voltage
F	The external force
J_i	The moment of inertia
K_g	The back electromotive force constant of the generator
LH	Left hip joint
LK	Left knee joint
$M_{(sub)}$	The mass of the subject
M_ι	The total external moment
P_g	The electricity power from the motor
P_{out}	The output power from the generator
R_o	The external resistive load
R_i	The internal resistance of the generator
$\ddot{S}_G$	The displacement vector of the subject's centre of gravity
μ	The gear ratio

References

1. WaterSafety-New-Zealand. Drowning Report 2020. Available online: https://drowningreport2020.watersafety.org.nz/ (accessed on 28 January 2021).
2. To, J.; Huang, L. Life jacket based energy harvesting to assist search and rescue-a review. In Proceedings of the 2022 17th International Conference on Control, Automation, Robotics and Vision (ICARCV), Singapore, 11–13 December 2022; pp. 925–930.
3. MacIver, K.; Asbury, E.; Mitchell, G.; van der Meulen, C.; Asbury, E.A. New Zealand Search and Rescue fatality data: Creating targeted prevention messaging. *J. Search Rescue* **2021**, *5*, 37–55. [CrossRef]
4. Water-Safety-New-Zealand. *New Zealand Water Safety Sector Strategy 2020*; Technical Report; Water-Safety-New-Zealand: Wellington, New Zealand, 2020.
5. Lee, K.Y.; Kim, S.B.; Kang, J.J.; Choi, S.J.; Choi, G.S.; Kang, E.Y. Positioning alarm system of smart life Jacket tube. *ARPN J. Eng. Appl. Sci.* **2018**, *13*, 1386–1390.
6. Gao, M.; Wang, P.; Jiang, L.; Wang, B.; Yao, Y.; Liu, S.; Chu, D.; Cheng, W.; Lu, Y. Power generation for wearable systems. *Energy Environ. Sci.* **2021**, *14*, 2114–2157. [CrossRef]
7. Yan, C.; Wang, J.; Lee, P.S. Stretchable graphene thermistor with tunable thermal index. *ACS Nano* **2015**, *9*, 2130–2137. [CrossRef] [PubMed]
8. Gong, S.; Schwalb, W.; Wang, Y.; Chen, Y.; Tang, Y.; Si, J.; Shirinzadeh, B.; Cheng, W. A wearable and highly sensitive pressure sensor with ultrathin gold nanowires. *Nat. Commun.* **2014**, *5*, 3132. [CrossRef] [PubMed]
9. Khan, Y.; Ostfeld, A.E.; Lochner, C.M.; Pierre, A.; Arias, A.C. Monitoring of vital signs with flexible and wearable medical devices. *Adv. Mater.* **2016**, *28*, 4373–4395. [CrossRef] [PubMed]
10. Silicon Labs. Energy Harvesting Reference Design. 2021. Available online: https://www.silabs.com/documents/public/application-notes/AN0021.pdf (accessed on 8 October 2024).
11. HopeRF. LoRa Modules and Products. 2024. Available online: https://www.hoperf.com/modules/lora/index.html (accessed on 8 October 2024).
12. Wu, F.; Rüdiger, C.; Redouté, J.M.; Yuce, M.R. WE-Safe: A wearable IoT sensor node for safety applications via LoRa. In Proceedings of the 2018 IEEE 4th World Forum on Internet of Things (WF-IoT), Singapore, 5–8 February 2018; pp. 144–148.
13. MacKenzie, J.D.; Ho, C. Perspectives on energy storage for flexible electronic systems. *Proc. IEEE* **2015**, *103*, 535–553. [CrossRef]
14. Deals New Zealand, M. Hutchwilco Easy-Fit Inflatable Life Jacket 170 N with ETS. Available online: https://www.marine-deals.co.nz/inflatable-life-jackets/hutchwilco-easy-fit-inflatable-life-jacket-170n-with-ets/ (accessed on 9 August 2022).
15. Jaycar. YG2734-dataSheetMain. 2017. Available online: https://www.jaycar.com.au/36rpm-12vdc-reversible-gearhead-motor/p/YG2734 (accessed on 8 October 2024).
16. To, J.; Huang, L. An Approach to Model Human Kinetic Energy Harvesting with Wearable Lifejackets to Assist Search and Rescue. In Proceedings of the 2023 5th International Conference on Electrical Engineering and Control Technologies (CEECT), Chengdu, China, 15–17 December 2023; pp. 370–374.
17. Univercity, A. Motion Capture Lab—About the facility. Available online: https://mocap.aut.ac.nz/facility (accessed on 8 October 2024).

18. Supanich, W.; Kulkarineetham, S.; Sukphokha, P.; Wisarnsart, P. Machine Learning-Based Exercise Posture Recognition System Using MediaPipe Pose Estimation Framework. In Proceedings of the 2023 9th International Conference on Advanced Computing and Communication Systems (ICACCS), Coimbatore, India, 17–18 March 2023; Volume 1, pp. 2003–2007.
19. Ismail, A.P.; Abd Aziz, F.A.; Kasim, N.M.; Daud, K. Hand gesture recognition on python and opencv. In Proceedings of the IOP Conference Series: Materials Science and Engineering, Mosul, Iraq, 5–6 April 2021; Volume 1045, p. 012043.
20. Bao, Y.; Fang, H.; Xu, J. Effects of currents on human freestyle and breaststroke swimming analyzed by a rigid-body dynamic model. *Machines* **2021**, *10*, 17. [CrossRef]
21. Bhamidipati, V.S.P.; Saxena, I.; Saisanthiya, D.; Retnadhas, M. Robust Intelligent Posture Estimation for an AI Gym Trainer using Mediapipe and OpenCV. In Proceedings of the 2023 International Conference on Networking and Communications (ICNWC), Chennai, India, 5–6 April 2023; pp. 1–7.
22. El-Hajj, M.; Mousawi, H.; Fadlallah, A. Analysis of lightweight cryptographic algorithms on iot hardware platform. *Future Internet* **2023**, *15*, 54. [CrossRef]
23. Hareedran, T.K. INA219 Current Sensor Module Primer. 2021. Available online: https://www.electroschematics.com/ina219-current-sensor-module-primer/ (accessed on 8 October 2024).
24. Bi, Z.; Zhang, W.; Chen, I.M.; Lang, S. Automated geneartion of the D–H parameters for configuration design of modular manipulators. *Robot. Comput. Integr. Manuf.* **2007**, *23*, 553–562. [CrossRef]